JOC The Journal of Organic Chemistry

UNIVERSITÉ PARIS SUD

Subscriber access provided by Bibliothèque de l'Université Paris-Sud

Article

Fluorophore-Labelling Tetraphenylethene Dyes Ranging From Visible to Near-Infrared Region: AIE Behavior, Performance in Solid State and Bioimaging in Living Cells

Weijie Chen, Chen Zhang, Xie Han, Sheng Hua Liu, Ying Tan, and Jun Yin

J. Org. Chem., **Just Accepted Manuscript** • DOI: 10.1021/acs.joc.9b01976 • Publication Date (Web): 16 Sep 2019

Downloaded from pubs.acs.org on September 17, 2019

Just Accepted

"Just Accepted" manuscripts have been peer-reviewed and accepted for publication. They are posted online prior to technical editing, formatting for publication and author proofing. The American Chemical Society provides "Just Accepted" as a service to the research community to expedite the dissemination of scientific material as soon as possible after acceptance. "Just Accepted" manuscripts appear in full in PDF format accompanied by an HTML abstract. "Just Accepted" manuscripts have been fully peer reviewed, but should not be considered the official version of record. They are citable by the Digital Object Identifier (DOI®). "Just Accepted" is an optional service offered to authors. Therefore, the "Just Accepted" Web site may not include all articles that will be published in the journal. After a manuscript is technically edited and formatted, it will be removed from the "Just Accepted" Web site and published as an ASAP article. Note that technical editing may introduce minor changes to the manuscript text and/or graphics which could affect content, and all legal disclaimers and ethical guidelines that apply to the journal pertain. ACS cannot be held responsible for errors or consequences arising from the use of information contained in these "Just Accepted" manuscripts.

is published by the American Chemical Society. 1155 Sixteenth Street N.W., Washington, DC 20036

Published by American Chemical Society. Copyright © American Chemical Society. However, no copyright claim is made to original U.S. Government works, or works produced by employees of any Commonwealth realm Crown government in the course of their duties.

Fluorophore-Labelling Tetraphenylethene Dyes Ranging From Visible to Near-Infrared Region: AIE Behavior, Performance in Solid State and Bioimaging in Living Cells

Weijie Chen[a, †], Chen Zhang[b, †], Xie Han[a, c, †], Sheng Hua Liu[a], Ying Tan[b*] and Jun Yin[a, b*]*

[a] Key Laboratory of Pesticide and Chemical Biology, Ministry of Education, Hubei International Scientific and Technological Cooperation Base of Pesticide and Green Synthesis, International Joint Research Center for Intelligent Biosensing Technology and Health, College of Chemistry, Central China Normal University, Wuhan 430079, China.

[b] State Key Laboratory of Chemical Oncogenomics, Key Laboratory of Chemical Biology, the Graduate School at Shenzhen, Tsinghua University, Shenzhen, Guangdong, PR China, 518055.

[c] School of Chemistry and Chemical Engineering, Wuhan University of Science and Technology, Wuhan 430081, China.

[†] These authors contributed equally to this work.

*Corresponding to: yinj@mail.ccnu.edu.cn ; tan.ying@sz.tsinghua.edu.cn ; Hanxie@wust.edu.cn

KEYWORDS: Tetraphenylethene, AIE, fluorophore, mechanoresponsive luminescence (MRL), bioimaging

ABSTRACT: Functional molecules with aggregation-induced emission (AIE) have lately received the most attention due to their versatile functions in many fields. In this work, tetraphenylethene (TPE) as one of the most concerned AIE systems was installed on different fluorophores including dansyl, naphthalimide, 4-nitro-1,2,3-benzoxadiazole (NBD), borondipyrromethene (BODIPY), hemicyanine to afford a series of new fluorescent dyes, whose spectra covered a fluorescence region of visible to near-infrared emission. Especially, these tetraphenylethene-containing compounds all exhibited AIE behavior. In solid state, they presented multicolor including blue, orange, red, crimson and NIR (near-infrared emission). It was worth mentioning that the dansyl- and NBD- coating TPEs exhibited obvious mechanoresponsive luminescence (MRL) phenomena. Moreover, these AIE-based TPEs displayed good bioimaging performance in living cells. This work will be helpful for designing functional AIE dyes with different fluorescence emission.

Introduction

With the rapid development of visualization and imaging technology, functional fluorescent dyes are of growing use in materials chemistry and biochemistry on the account of their marvelous applications in organic semiconductors, fluorescent probes, chemosensors, bioimaging, diseases diagnosis and therapy etc.[1-16] To gain the fluorescent dyes with high performance, one of the biggest challenges is that the dyes need to overcome the effect of fluorescence weakening or quenching caused by molecular aggregation.[17-22] As an opposite of aggregation caused quenching (ACQ), the aggregation-induced emission (AIE)-active fluorescent dyes can weaken the influence

of molecular aggregation. Over past several years, a large number of AIE molecules with various function have been developed and applied in the fluorescence-related fields.[23-28] For instance, their high performance in solid state or thin film can be used to construct the stimuli-responsive fluorescent sensors while their excellent behavior in aqueous can serve as the biomaterials to be applied in bioimaging of living systems.[29] Accordingly, exploring the multi-functional AIE-active fluorescent dyes is vitally significant for promoting the development of imaging technology and meeting the requirements of fluorescent dyes suitable for different imaging scenes.

Tetraphenylethene (TPE), as the classic AIE-based molecular backbone, has been widely used to construct the stimuli-responsive fluorescent sensors and bioimaging materials with AIE performance by many groups.[30] In our group, we employed the TPE backbone as a building block to construct a series of fluorescent sensors and fluorescent probes in recent years.[29, 31-32] In consideration of the fact that these fluorescent TPEs were mainly in narrow region of spectra emission and some TPEs were non-AIE active, we reported a series of AIE-based fluorescent dyes ranging from visible to near-infrared region by fusing TPE moiety and different fluorophores including dansyl, naphthalimide, 4-nitro-1,2,3-benzoxadiazole (NBD), borondipyrromethene (BODIPY), hemicyanine in **Scheme 1**, and detailedly investigated their AIE behavior, performance in solid state and bioimaging application.

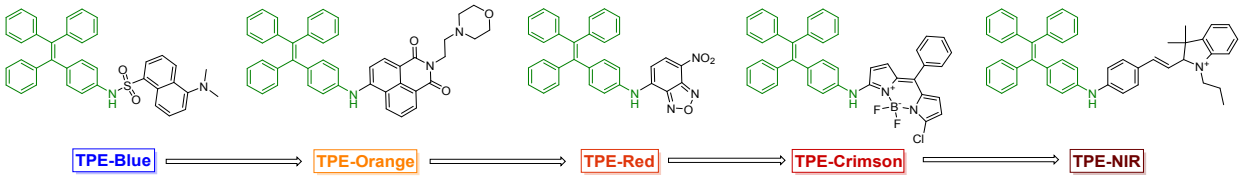

Scheme 1 The molecular structures of TPEs ranging from visible to near-infrared region.

Results and discussion

Synthesis and structural details of TPEs. The TPEs were synthesized through the reaction of TPE-based amine **1** with corresponding halogen-containing fluorophores, as outlined in **Scheme 2**. **TPE-Blue** was synthesized by the treatment of amine **1** and dansyl chloride **2** while **TPE-Orange** was obtained by employing naphthalimide-based bromide **3**[33] as a starting material to carry out a coupling reaction of carbon-nitrogen bond formation with **1** in presence of $Pd(OAc)_2$. The nucleophilic substitution of amine **1** with chlorides **4** and **5**[34], respectively, generated the corresponding **TPE-Red** and **TPE-Crimson**. While **TPE-NIR** was obtained via the condensation between 2,3,3-trimethyl-1-propyl-3H-indol-1-ium iodide **8**[35] and TPE-based aldehyde **7** that was prepared by a similar Pd-catalyzed coupling reaction of amine **1** with bromide **6**. All new intermediates and targeting molecules were well characterized by ^{1}H NMR, ^{13}C NMR and mass spectroscopies (see **Figure S7-S20** in Supporting Information).

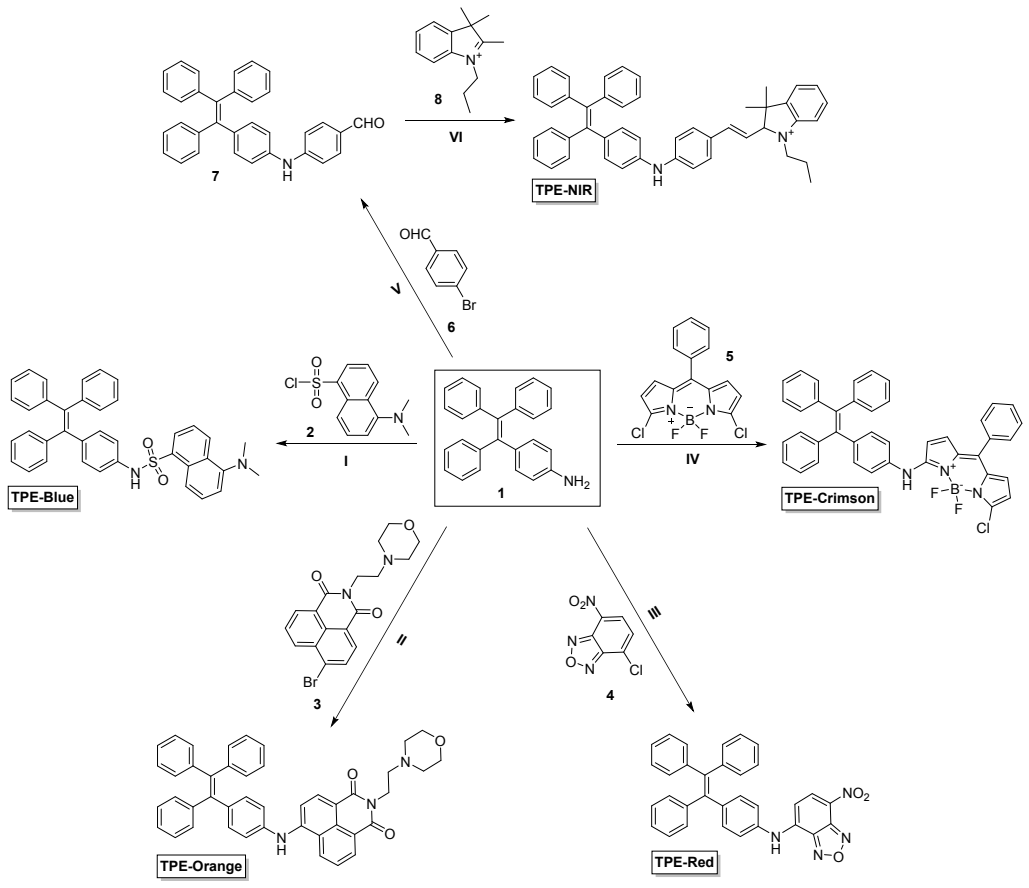

Scheme 2 The synthesis of the multi-color TPE derivatives. I) NEt_3, DCM, R.T, 12 h, 65%. II) K_2CO_3, $Pd(OAc)_2$, toluene, 100 ℃, 12 h, 64%. III) NEt_3, MeCN, reflux, 12 h, 51%. IV) NEt_3, 1,4-dioxane, 80 ℃, 12 h, 45%. V) Cs_2CO_3, $Pd(dba)_2$, BINAP, toluene, 100 ℃, 16 h, 60%. VI) Pyridine, ethanol, 60 ℃, 12 h, 70%. (NEt_3: triethylamine, DCM: dichloromethane, R.T: room temperature, BINAP: (±)-2,2'-Bis(diphenylphosphino)-1,1'-binaphthalene)

Further efforts paid for seeking more details of molecular structures by X-ray single crystal diffraction. Fortunately, the single crystals of **TPE-Blue** and **TPE-NIR** suitable for crystallographic analysis were obtained by slow diffusion of hexane into a CH_2Cl_2 solution of **TPE-Blue** and **TPE-NIR** at room temperature, respectively. The corresponding crystallographic data and thermal ellipsoid plots were summarized in **Table S2, Figure S1** and **S2** in Supporting Information. From the crystal structure of **TPE-Blue** illustrated in **Figure 1A**, it was found that

TPE component and dansyl-amide framework presented almost vertical configuration. And there were multiple weak intermolecular interactions between molecules, including N-H···O (**Figure 1B**), C-H···N (**Figure 1C**), C-H···O (**Figure 1D**), and C-H···π (**Figure 1E**) interactions. Such multi-interaction resulted that the fluorescent dye in crystalline phase presented highly ordered stacking, as shown in **Figure 1F**. In which, the TPE components and naphthalene rings were arranged in an alternating herringbone manner.

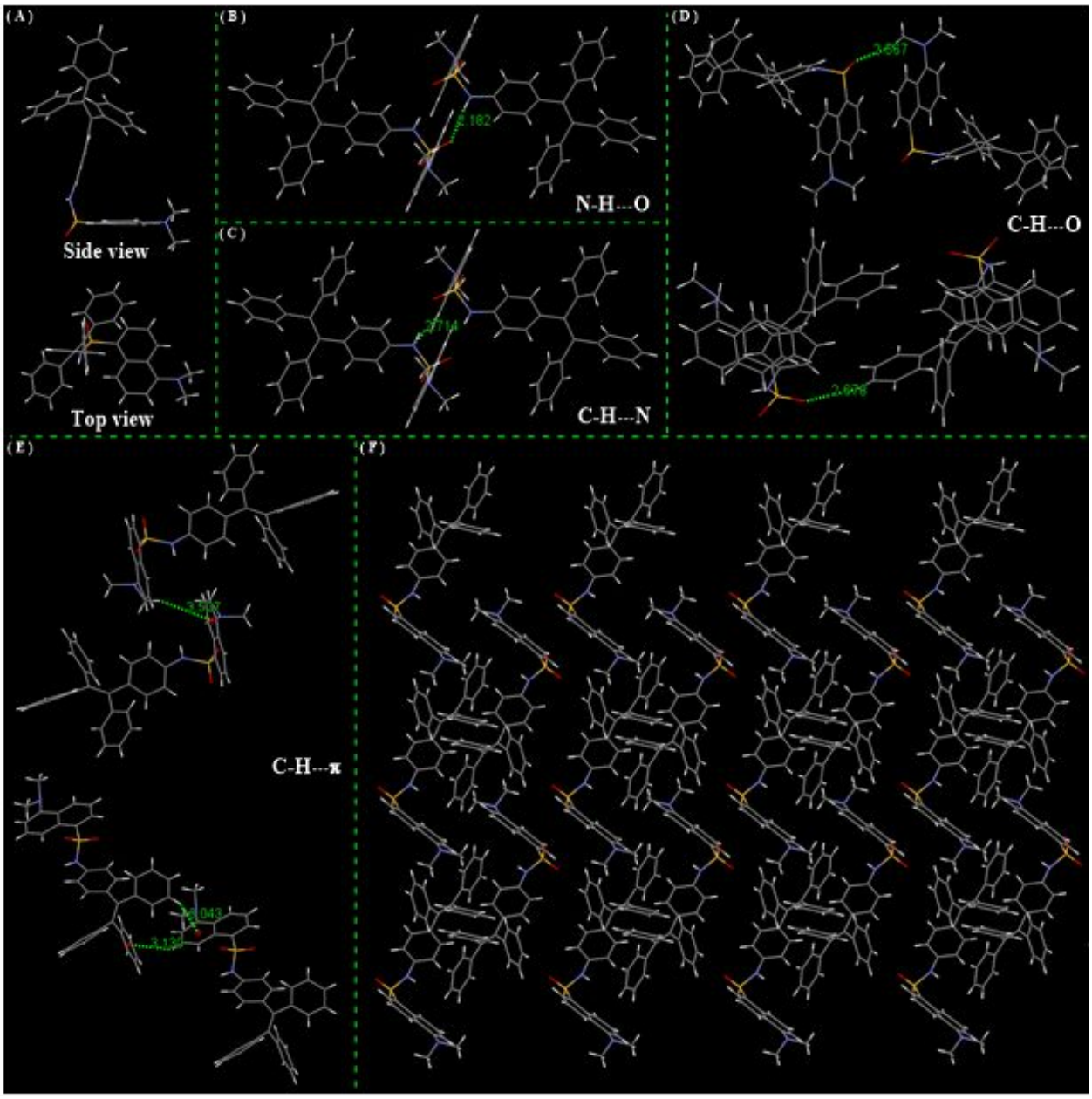

Figure 1 The single crystal structure (A), N-H···O interaction (B), C-H···N interaction (C), C-H···O interaction (D), C-H···π interaction (E) and the stacking view (F) of dye **TPE-Blue**.

According to the crystal structure of dye **TPE-NIR** in **Figure 2A**, TPE component showed similar twisted configuration as well as dye **TPE-Blue** while the hemicyanine moiety exhibited a planar structure. Analyzing the intermolecular interactions found that it mainly involved in three weak interactions such as C-H···π interaction (**Figure 2B**) and N-H···N interaction (**Figure 2C**).

In stacking view of **TPE-NIR**, the intermolecular hemicyanine components were arranged to a face-to-face pattern, the distance of two aromatic centers is up to 3.925 Å **(Figure 2D**) owing to the large space steric hindrance of TPE.

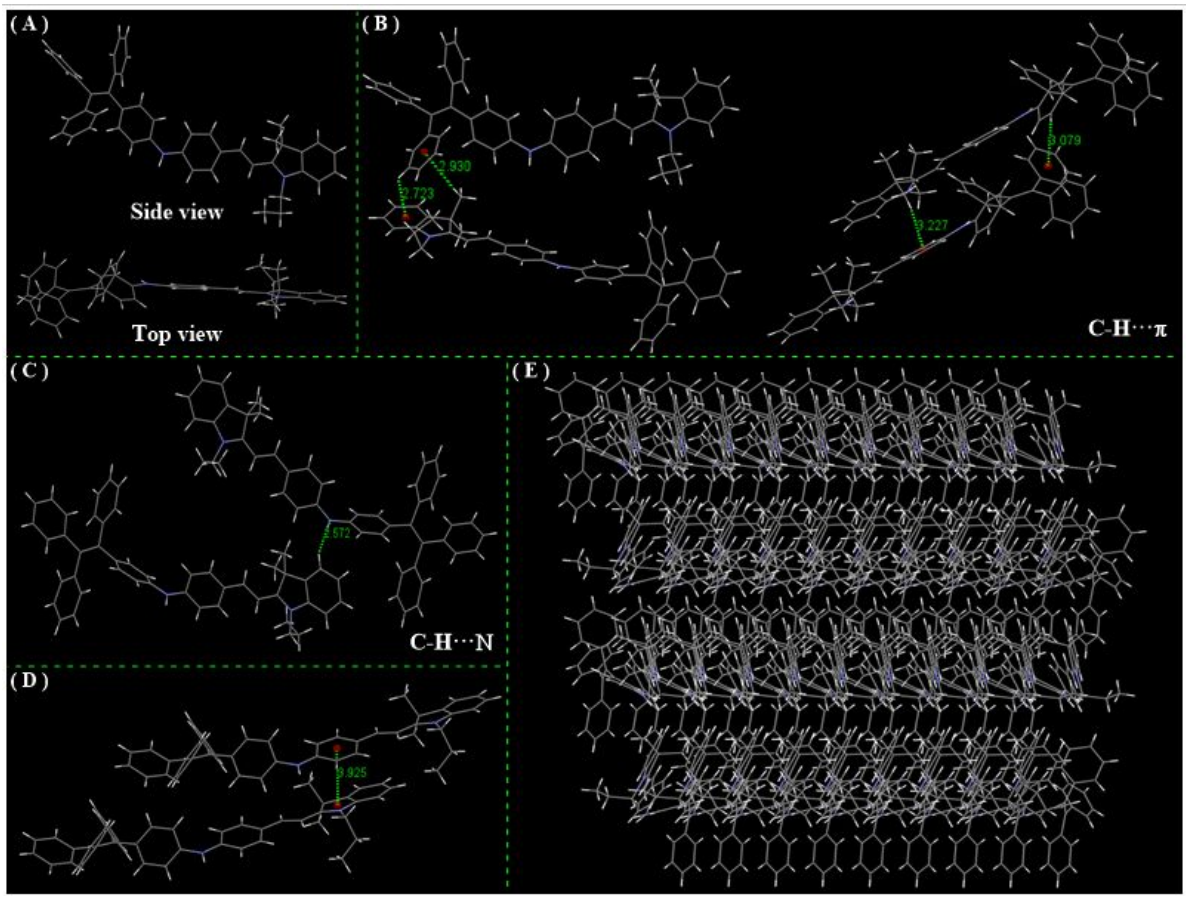

Figure 2 The single crystal structure (A), C-H···π interaction (B), C-H···N interaction (C), centers distance (D) and the stacking view (E) of dye **TPE-NIR**.

To gain insight into the electronic properties of TPEs, time-dependent density functional theory (TD-DFT) calculations were carried out at the B3LYP/6-31G* level with the Gaussian 09 program to explore their frontier molecular orbitals and electronic transitions upon photoexcitation.[36] The maximum absorption and corresponding molecular orbitals for these major electronic transitions were shown in **Figure 3**. The optimized structure of **TPE-Blue** in **Figure 3A** exhibited a similar

configuration with single crystal. The result of the absorption spectrum showed that **TPE-Blue** involved in a main S_0-S_2 electronic transition (around 350 nm) with a large oscillator strength of 0.5166, corresponding to 57% contribution from the HOMO to LUMO+1 transition (**Table S3** in Supporting Information). More, its electron density of the highest occupied molecular orbital (HOMO) was distributed in TPE moiety while the lowest unoccupied molecular orbital (LUMO) was mainly localized on the dansyl-amide backbone. For dye **TPE-Orange**, it contained three main absorption bands at around 482, 380 and 353 nm, respectively, as shown in **Figure 3B**. The distribution of HOMO mainly focused on the morpholine ring while the LUMO was distributed in naphthalimide fluorophore. Similar three absorption bands (at 560, 418 and 350 nm, respectively) with large oscillator strengths were also observed in molecule of **TPE-Red** in **Figure 3C**. Differently, its electron density of HOMO mainly distributed in TPE unit while LUMO was located in NBD backbone. For BODIPY- and hemicyanine-cotaining **TPE-Crimson** and **TPE-NIR**, they involved in multi-electronic transitions, as shown in in **Figure 3D** and **Figure 3E**. Especially, the HOMO and LUMO electron density of all molecules had the charge transfer characteristics, which implied that these dyes were probably fluorescent.[37] Additionally, investigation on the energy levels (such as 3.81, 2.99, 2.72, 2.45 and 1.63 eV, respectively) found that they possessed a trend of decreasing band gaps, suggesting that their optical behavior had gradual red-shift.

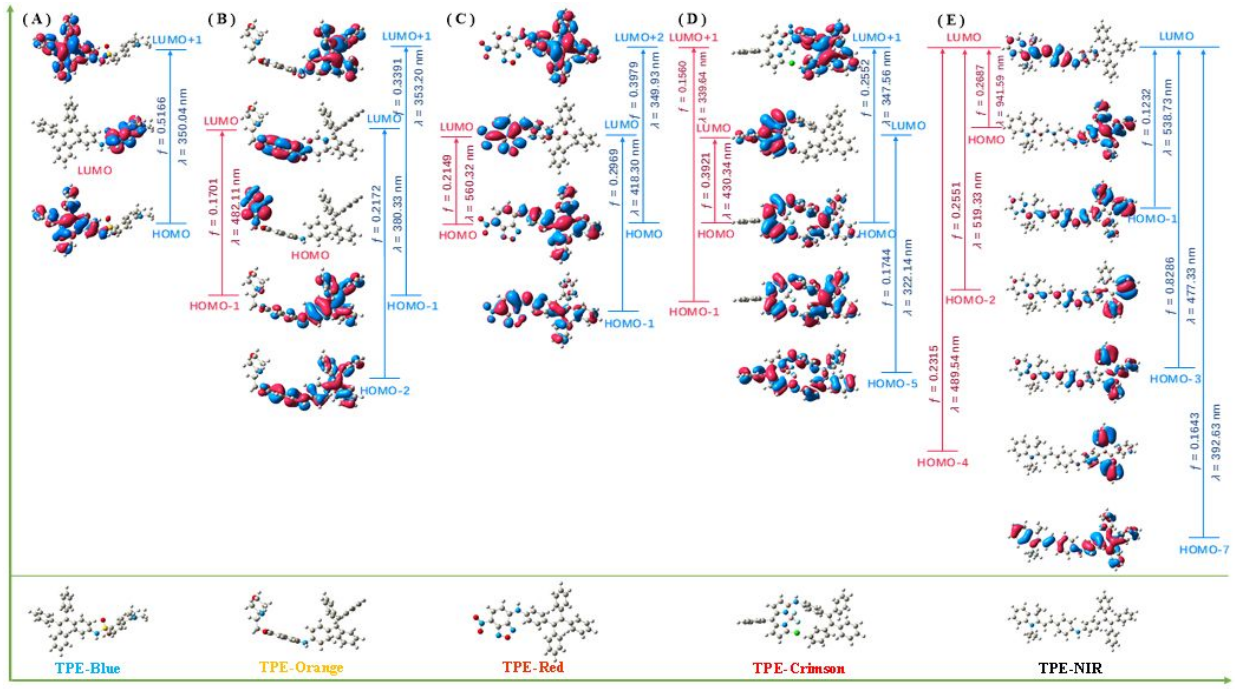

Figure 3 Frontier molecular orbital profiles of (A) **TPE-Blue**, (B) **TPE-Orange**, (C)**TPE-Red**, (D)**TPE-Crimson** and (E) **TPE-NIR** based on TDDFT (B3LYP/6-31G*) calculations.

AIE behavior. As known, TPE backbone has been widely applied in the construction of AIE-based functional materials. In consideration of these molecules containing TPE unit, the subsequent work focused on investigating their AIE behavior by UV-Vis absorption and fluorescence spectra at room temperature. All measurements were carried out in a solution of MeCN/H_2O with different volume fractions of water (f_w). Except for **TPE-Blue** (around at 220-400 nm) with sulfonamide moiety, the UV-Vis absorption spectra of **TPE-Orange**, **TPE-Red**, **TPE-Crimson** and **TPE-NIR** exhibited the main absorption band peaked at 450, 485, 497 and 537 nm (**Figure S3** in Supporting Information), respectively. With increasing volume fractions of water, no significant changes were observed (**Figure S3** in Supporting Information).

Subsequently, their AIE behavior was clearly demonstrated in their fluorescence spectra. As shown in **Figure 4A**, the emission peaks of **TPE-Blue** exhibited a complicated solvatochromic

shift. In pure MeCN, **TPE-Blue** showed a yellow-green fluorescence around at 519 nm with the absolute fluorescence quantum yield of 23%. Along with increasing the water fractions from 0 to 60%, its fluorescence red-shifted gradually to 538 nm emitting yellow emission and the absolute fluorescence quantum yield displayed a slight reduction (Φ_f = 17%). The red shift was mainly due to the intramolecular charge transfer (ICT) effect in response to the increasing solvent polarity of the mixture solution. When the water fractions increased to over 60%, the emission intensity of **TPE-Blue** increased gradually with the increase of water fractions. Simultaneously, the emission peak blue-shifted to 497 nm and presented a green emission with enhanced fluorescence quantum yields of 28% when the water fractions were up to 90% in **Figure 4F**, probably owing to the formation of its aggregation, which restricted the intermolecular and intramolecular interactions and led to higher energy emission.[38-39] These observations were well consistent with the findings of the previous work.

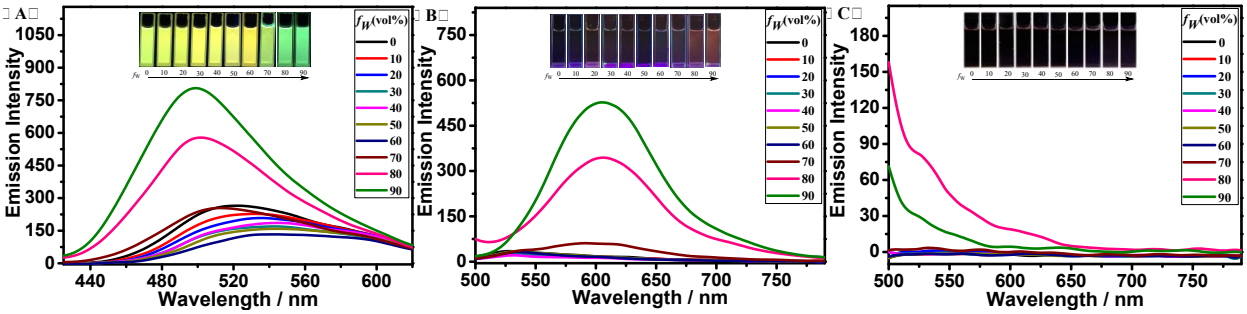

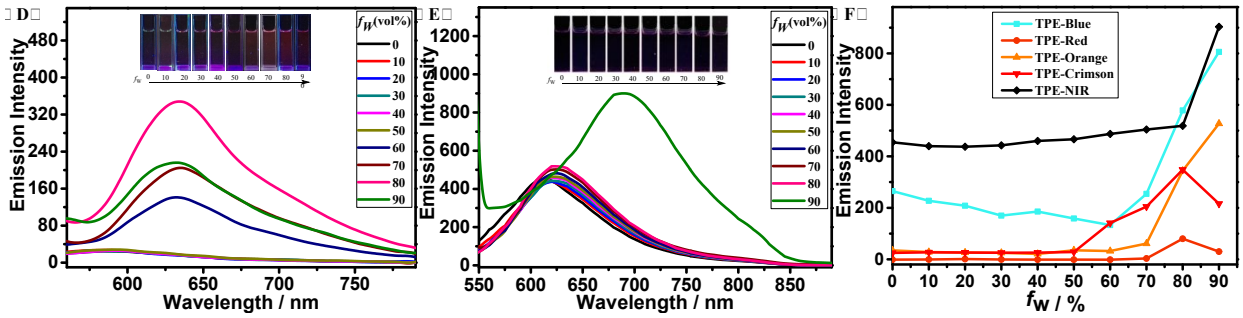

Figure 4 The fluorescence spectra of compounds (10 μM) **TPE-Blue** (A), **TPE-Orange** (B), **TPE-Red** (C), **TPE-Crimson** (D) and **TPE-NIR** (E) in MeCN/H_2O mixtures with different water fractions.

For the naphthalimide-containing fluorescent dye, **TPE-Orange** was non-fluorescent in pure MeCN and its fluorescence intensity in mixture solution of MeCN-H_2O showed few changes when the water fractions were in range of 0-60% (Φ_f = 0.4% in MeCN), as presented in **Figure 4B**. However, a dramatic enhancement of the fluorescence intensity at 606 nm was observed when the water fractions changed from 70% to higher water fraction (90%, Φ_f = 1.5%) in **Figure 4F**, which strongly suggested that **TPE-Orange** had typical AIE activity. In contrast, no traditional AIE phenomenon was found when the NBD-based dye **TPE-Red** was carried out the same operation (**Figure 4C** and **Figure 4F**), probably ascribing to the fact dye **TPE-Red** was difficult to form the corresponding aggregation under the condition of MeCN-H_2O solution. Similar to **TPE-Orange**, the BODIPY-bearing dye **TPE-Crimson** revealed a typical AIE character. As described in **Figure 4D**, few changes of its fluorescence intensity in mixture solution of MeCN-H_2O was detected on the f_w range of 0-50% (Φ_f = 0.3% in MeCN). Subsequently, a dramatic enhancement of the fluorescence was observed at higher water fractions (60-90%) and the fluorescence intensity peaked at 633 nm reached a maximum when the water fraction was 80% (Φ_f = 1.2%) in **Figure 4F**. In comparison to the above, the hemicyanine-moidified near-infrared dye **TPE-NIR** exhibited a different AIE behavior. As could be found in **Figure 4E**, **TPE-NIR** showed an obvious

fluorescence emission at 622 nm in pure organic solvent and the fluorescence intensity in MeCN-H_2O displayed slight enhancement when the water fractions were in range of 0-80% (Φ_f= 0.4% in MeCN). However, its fluorescence red-shifted to 690 nm the f_w was up to 90% (Φ_f= 0.9%) in **Figure 4F**. These results strongly indicated that the introducing fluorophores was able to adjust their fluorescence emission while the TPE unit might affect their AIE activity. For the reason, we speculated that their AIE activity probably originated from the combination of ICT/TICT effect and restricted intramolecular rotation (RIR) according to the above observations and the solvatochromic properties (**Figures S4** and **S5** in Supporting Information). More, the further proof was found when we measured their fluorescence spectra in mixture solutions of glycerol/methanol with different viscosity (**Figure S6** in Supporting Information). Especially for dye **TPE-Red**, its emission intensity gradually increased with the enhancement of viscosity of solvent due to the RIR process (**Figure S6C** in Supporting Information), which confirmed dye **TPE-Red** was AIE-activated.

Performance in solid state. To further confirm the AIE activity of these fluorescent dyes, we investigated their fluorescence property in solid state. As presented in **Figure 5A**, the emission peaks of **TPE-Blue**, **TPE-Orange**, **TPE-Red**, **TPE-Crimson** and **TPE-NIR** centered at 470, 611, 660, 665 and 722 nm, respectively, and ranged from visible to near-infrared region, as observed from the images of their powder in **Figure 5B**. It was particularly worth mentioning that dye **TPE-Red** revealed a bright red emission in solid state in comparison to its non-emissive behavior in solution. The result strongly indicated that **TPE-Red** was also an AIE-active fluorescent dye. Further proof was achieved by checking their absolute fluorescent quantum yields in solid state which were 57%, 3.2%, 1.5%, 2.5% and 1.4% of **TPE-Blue**, **TPE-Orange**, **TPE-Red**, **TPE-Crimson** and **TPE-NIR**, respectively. According to the data, it was found that they had higher

fluorescent quantum yields in solid state than in solution, which completely verified that these fluorophore-labelling TPEs had typical AIE behavior and their emission ranged from visible to near-infrared emission.

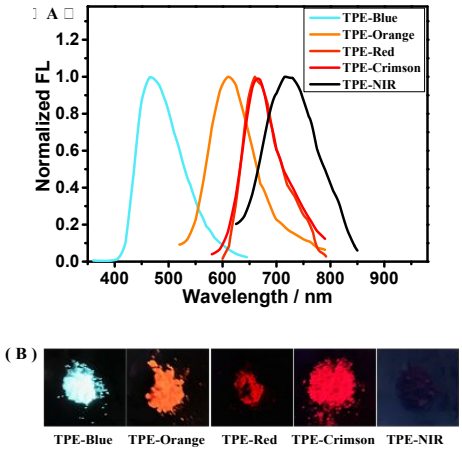

Figure 5 The fluorescence spectra (A) and the emission images under 365 nm (B) of the TPEs in solid state.

For TPEs, numerous studies have confirmed that they possessed mechanically responsive performance in powder.[40-47] Accordingly, subsequent studies were conducted to explore their mechanically induced fluorescence performance in solid state. The results showed that the dansyl-based **TPE-Blue** and NBD-based **TPE-Red** exhibited mechanoresponsive properties in comparison to others (**Figure 6)**. The as-prepared pristine **TPE-Blue** exhibited a strong blue emission at 470 nm. By mechanically grinding the powder of **TPE-Blue** using a pestle, an obvious bathochromic emission at 492 nm was observed in **Figure 6A**. As a result of grinding, the absolute fluorescence quantum yields increased largely from 57% to 78% with the changes of image color from blue to bright green in **Figure 6B**. Interestingly, the bright blue emissions of the solid powder was able to be fully recovered by fuming it with dichloromethane or heating it to 150 ℃ for 3 min after the grinding process, suggesting that **TPE-Blue** had a reversible mechanochromic behavior. To gain insight into the mechanism of mechanochromism process, we collected the powder X-ray

diffractions (PXRD) spectra of the as-prepared, ground and the fumed/annealed **TPE-Blue** solids. In **Figure 6C**, the spectrum of the as-prepared **TPE-Blue** had many sharp diffraction peaks, implying the crystalline characteristic. In contrast, these sharp peaks almost disappeared upon mechanically grinding, indicating that mechanical grinding changed the stacking of **TPE-Blue** from the crystalline phase to the amorphous phases. Moreover, and the original crystalline state can be regained by exposure to CH_2Cl_2 vapor or heating. These observations demonstrated that the morphology transition between the crystalline and amorphous states was responsible for the mechanochromism of **TPE-Blue**.

In comparison to the bathochromic emission of **TPE-Blue**, **TPE-Red** exhibited a different mechanoresponsive behavior. The as-prepared sample of **TPE-Red** showed a strong red emission at 660 nm (In **Figure 6D**). Upon mechanically grinding, the bright red emission decreased dramatically with the changes of fluorescent quantum yields from 1.7% to 0.6%. Similar solvent fuming or thermal annealing can lead to a fully recovery of the red emission in **Figure 6E**. Likewise, the process of crystalline-to-amorphous state transitions was able to be confirmed by the PXRD in **Figure 6F**.

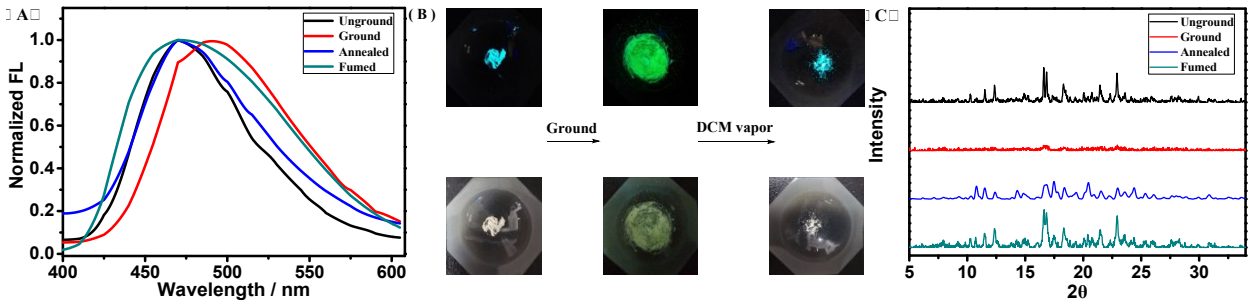

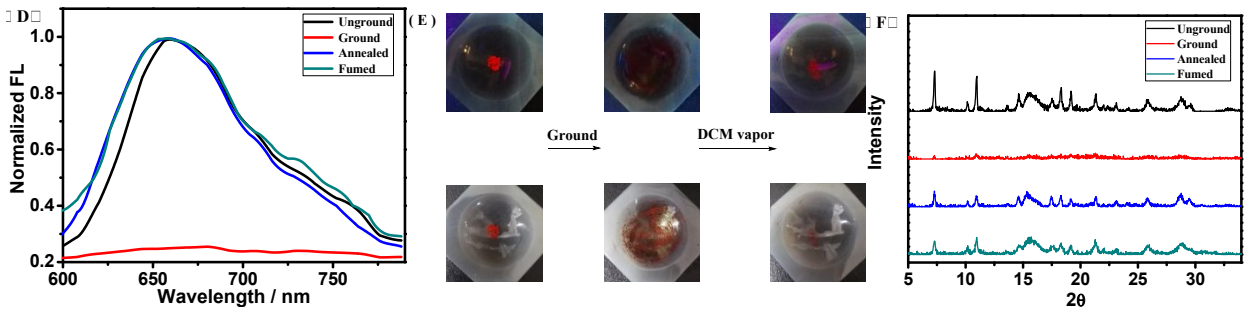

Figure 6 The MRL performance of **TPE-Blue** and **TPE-Red**. (A, D) The fluorescence spectra in solid state; (B, E) Images under 365 nm UV irradiation (up) and daylight (down) of the as-prepared, ground and fumed samples; (C, F) The XRD spectra.

Bioimaging in living cells. On account of the fact that these TPE-containing fluorescent dyes all exhibited AIE activity and nearly covered the broad emission region from the visible channel to NIR channel, we attempted to apply them in bioimaging of live cells. Accordingly, HeLa cells were cultured in Dulbecco's modified Eagle's Medium (DMEM) supplemented with 10% fetal bovine serum (FBS) and then incubated at 37 ℃ under a humidified atmosphere containing 5% CO_2. The cells were washed with ice-cold PBS three times and then incubated with fresh culture medium. The solution (10 μM) of dyes **TPE-Blue**, **TPE-Orange**, **TPE-Red**, **TPE-Crimson** and **TPE-NIR**, respectively, was prepared in phosphate buffered saline (PBS, pH = 7.4) containing 0.1% DMSO at 37 ℃. After incubating with HeLa cells for 0.5-4 h and then washing these cells with PBS, the fluorescence images were collected using a confocal microscope. As could be observed by viewing the confocal fluorescence microscope images shown in **Figure 7**, a series of bright emission was able to be detected and presented multi-color character. These findings strongly indicated that the AIE-active TPEs can serve as the tracking tools to be applied in bioimaging.

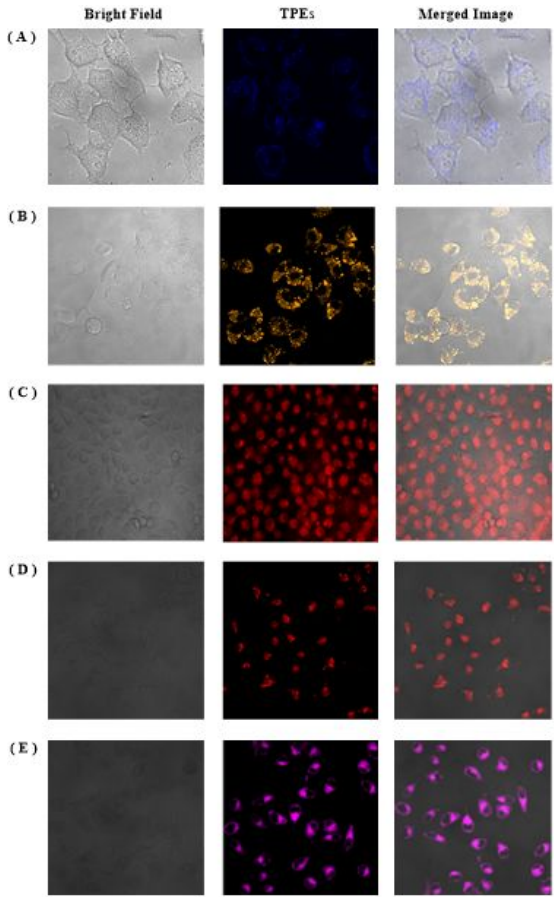

Figure 7 The confocal images of Hela cells in different emission channels with **TPE-Blue** (A), **TPE-Orange** (B), **TPE-Red** (C), **TPE-Crimson** (D) and **TPE-NIR** (E) (The near-infrared fluorescence was modified graphically to purple for visual clarity).

Conclusions

In summary, a series of new AIE systems, installing TPE on different fluorophores (dansyl, naphthalimide, NBD, BODIPY, hemicyanine) were developed, with fluorescent spectra bands covering the region from visible to near-infrared emission, showing multicolors including blue, orange, red, crimson and NIR. Though the way of charge transfer, different coated blocks resulted in the varied AIE behaviors. Surprisingly, the dansyl- and NBD-coating TPEs showed up obvious MRL phenomena which were ascribed to the morphology transitions. Moreover, great staining

performances in living cell were exhibited in these TPEs, implying a feasible method to construct new functional AIE dyes with diverse optical properties. Our study provided a kind of design strategy involving in ICT/TICT and RIR processes to construct the AIE functional materials with multicolour through installing different fluorophores on TPE backbone.

Experimental Section

Genenal. All reactions were carried out under a nitrogen atmosphere by using standard Schelenk techniques. All starting materials were obtained commercially as analytical grade and the solvents were used with dehydration and degassing purification. The compound **1** was a known structure, and **3**, **5** and **8** were synthesized according to the reported literatures.

^{1}H and ^{13}C NMR spectra were collected on an American Varian Mercury Plus 400/600 spectrometer (400/600 MHz) and used tetramethylsilane as the internal reference. Mass spectra were recorded with an EI mass spectrometer. Elements analysis were measured by a Vario ElIII Chnso analyzer. UV/Vis spectra were recorded by using a Hitachi U-3310 visible recording spectrophotometer. Fluorescence spectra were recorded by using a Hitachi-F-4500 instrument. Crystal structures were obtained on a Bruker APEX DUO charge-coupled device (CCD) system through single crystal XRD experiments. Intensity data were collected on a Nonius Kappa CCD diffractometer with Cu Kα radiation (λ = 1.54 Å) at room temperature. The structures were solved by a combination of direct methods (SHELXS-97) and Fourier difference techniques and refined by a full-matrix least-squares process (SHELXL-97). All non-hydrogen atoms were refined anisotropically. Data on the structures reported here had been deposited with the Cambridge Crystallographic Data Centre with deposition numbers CCDC 1937424 and 1937425. The

hydrogen atoms were placed in ideal positions and refined as riding atoms. The quantum chemistry calculation was performed on the Gaussian 03W (B3LYP/6-31G* basis set) software package.

Synthesis of Compound 1 (1-(4-Aminophenyl)-1,2,2-triphenylethene). The Zn powders (14.8 g, 229 mmol) was added to a 250 mL two-necked flask, followed by the addition of dry THF (80 mL) under a nitrogen atmosphere. The reactants were cooled to 0-5 ℃, stirred for 0.5 h at room temperature after the $TiCl_4$ (21.0 g, 114.5 mmol) was added dropwise, then reflux for 2.5h. After that, the reactants were cooled to 0-5 ℃ again, stirred for 10 min at room temperature after the pyridine (4.5 g, 57.25 mmol) was added dropwise. Then benzophenone (5.0 g, 27.4 mmol) and 4-aminobenzophenone (4.5 g, 22.9 mmol) in THF (50 mL) were then added dropwise, and reflux for 24 h. The mixture was poured into saturated sodium carbonate solutions. The residue was filtered and washed with ethyl acetate. The combined organic layers were washed with water and brine, dried over anhydrous Na_2SO_4, and evaporated under vacuum to afford **1**, which was purified by means of column chromatography, as a yellow solid (5.8 g, 74%).

Synthesis of Compound 7 (4-((4-(1,2,2-triphenylvinyl)phenyl)amino)benzaldehyde). The **1** (100 mg, 0.29 mmol) and **6** (63.9 mg, 0.35 mmol), Cs_2CO_3 (6.6 mg, 1.06% mmol), $Pd(dba)_2$ (2.0 mg, 0.35% mmol), BINAP (140 mg, 0.43 mmol) were dissolved in 10 mL dry toluene under a nitrogen atmosphere. The reactants were stirred at 100 ℃ for 16 h. The mixture was then poured into aqueous solution of ammonia and extracted with dichloromethane (3 x 20 mL). The combined organic layers were washed with water and brine, dried over anhydrous Na_2SO_4, and evaporated under vacuum to afford **7**, which was purified by means of column chromatography, as a light-yellow solid (78 mg, 60%). ^{1}H NMR (600 MHz, $CDCl_3$): δ (ppm) = 9.78 (s, 1H), 7.73 (d, J = 6 Hz, 2H), 7.05-6.92 (m, 21H), 6.12 (s, 1H). $^{13}C\{^1H\}$ NMR (150 MHz, DMSO-d_6): δ (ppm) = 187.6, 146.7, 141.1, 140.9, 138.2, 137.5, 136.5, 135.6, 129.8, 129.4, 128.7, 125.8, 125.1, 125.0, 123.8,

123.8, 117.2, 112.0, 106.0. EI-MS: m/z = 451.10 $[M]^+$; calculated exact mass: 451.19. Anal. Calcd. for $C_{33}H_{25}NO$: C, 87.77; H, 5.58; N, 3.10. Found: C, 87.62; H, 5.71; N, 3.22.

Synthesis of TPE-Blue (5-(dimethylamino)-N-(4-(1,2,2-triphenylvinyl)phenyl)naphthalene-1-sulfonamide). The **1** (0.10 g，0.29 mmol) and **2** (0.11 g, 0.43 mmol) were dissolved in 30 mL dry dichloromethane, followed by the addition of Et_3N (0.2 mL) under a nitrogen atmosphere. The reactants were stirred at room temperature for 12 h. The mixture was then evaporated and the residue was dissolved in dichloromethane and extracted (3 x 20 mL). The combined organic layers were washed with water and brine, dried over anhydrous Na_2SO_4, and evaporated under vacuum to afford **TPE-Blue**, which was purified by means of column chromatography, as a white solid (0.10 g, 65%). ^1H NMR (400 MHz, $CDCl_3$): δ (ppm) = 8.52(d, *J* = 8 Hz, 1H), 8.29 (d, *J* = 8 Hz, 1H), 8.08 (d, *J* = 8 Hz, 1H), 7.57 (t, *J* = 8 Hz, 1H), 7.43 (t, *J* = 10 Hz, 1H), 7.19 (d, *J* = 8 Hz, 1H), 7.06-6.89 (m, 15H), 6.76(d, *J* = 8 Hz, 2H), 6.63(d, *J* = 8.0 Hz, 2H), 6.53 (s, 1H), 2.89 (s, 6H).$^{13}C\{^1H\}$ NMR (150 MHz, $CDCl_3$): δ (ppm) = 152.0, 143.3, 141.0, 140.7, 139.8, 134.5, 133.9, 132.0, 131.2, 130.7, 130.4, 129.7, 128.6, 127.6, 126.4, 123.0, 120.8, 118.5, 115.2, 45.4. EI-MS: m/z = 580.18 $[M]^+$; calculated exact mass: 580.22. Anal. Calcd. for $C_{38}H_{32}N_2O_2S$: C, 78.59; H, 5.55; N, 4.82. Found: C, 78.70; H, 5.69; N, 4.73.

Synthesis of TPE-Orange (2-(2-morpholinoethyl)-6-((4-(1,2,2-triphenylvinyl)phenyl)amino)-1H-benzo[de]isoquinoline-1,3(2H)-dione). The **1** (66 mg, 0.19 mmol), **3** (50 mg, 0.13 mmol), K_2CO_3 (70 mg，0.51 mmol), $Pd(OAc)_2$ (57 mg，0.26 mmol)were dissolved in 10 mL dry toluene under a nitrogen atmosphere. The reactants were stirred at 100 ℃ for 12 h. The mixture was then evaporated and the residue was dissolved in dichloromethane and extracted (3 x 20 mL). The combined organic layers were washed with water and brine, dried over anhydrous Na_2SO_4, and

evaporated under vacuum to afford **TPE-Orange**, which was purified by means of column chromatography, as an orange solid (54 mg, 64%). ^{1}H NMR (600 MHz, $CDCl_3$): δ (ppm) = 8.61 (d, *J* = 6 Hz, 1H), 8.40 (d, *J* = 12 Hz, 1H), 8.25 (d, *J* = 6 Hz, 1H), 7.69 (t, *J* = 6 Hz, 1H), 7.28 (s, 1H), 7.21-6.88 (m, 18H), 6.75 (s, 1H), 4.33 (t, *J* = 7.0 Hz, 2H), 3.70 (s, 4H), 2.66 (d, *J* = 56.2 Hz, 6H). ^{13}C{^{1}H} NMR (100 MHz, $CDCl_3$): δ (ppm) = 164.50, 163.86, 146.46, 143.8, 143.5, 143.5, 141.3, 140.4, 140.1, 138.0, 133.5, 132.8, 131.4, 131.4, 131.3, 129.9, 127.8, 127.7, 126.7, 126.6, 126.6, 126.5, 125.5, 123.2, 121.9, 121.3, 113.2, 109.2, 67.1, 56.3, 53.9, 37.1. EI-MS: m/z = 655.07 $[M]^+$; calculated exact mass: 655.28. Anal. Calcd. for $C_{44}H_{37}N_3O_3$: C, 80.59; H, 5.69; N, 6.41. Found: C, 80.41; H, 5.88; N, 6.56.

Synthesis of TPE-Red (7-nitro-N-(4-(1,2,2-triphenylvinyl)phenyl)benzo[c][1,2,5]oxadiazol-4-amine). The **1** (0.35 g, 1 mmol) and **4** (0.20 g, 1 mmol) and were dissolved in 30 mL dry MeCN, followed by the addition of Et_3N (0.1 mL) under a nitrogen atmosphere. The reactants were stirred for reflux for 12 h. The mixture was then evaporated and the residue was dissolved in dichloromethane and extracted (3 x 20 mL). The combined organic layers were washed with water and brine, dried over anhydrous Na_2SO_4, and evaporated under vacuum to afford **TPE-Red** which was purified by means of column chromatography, as a red solid (0.26 g, 51%). ^{1}H NMR (400 MHz, $CDCl_3$): δ (ppm) = 8.42 (d, *J* = 8 Hz, 1H), 7.65 (s, 1H), 7.12-7.02 (m, 19H), 6.66 (d, *J* = 8 Hz, 1H). ^{13}C{^{1}H} NMR (150 MHz, $CDCl_3$): δ (ppm) = 144.7, 143.7, 143.2, 143.0, 143.0, 142.7, 142.0, 140.4, 139.4, 135.9, 134.5, 132.8, 131.2, 131.2, 131.1, 127.8, 127.6, 126.7, 126.6, 125.4, 122.1, 101.0. EI-MS: m/z = 510.13 $[M]^+$; calculated exact mass: 510.17. Anal. Calcd. for $C_{32}H_{22}N_4O_3$: C, 75.28; H, 4.34; N, 10.97. Found: C, 75.40; H, 4.27; N, 10.79.

Synthesis of TPE-Crimson (7-chloro-5,5-difluoro-10-phenyl-N-(4-(1,2,2-triphenylvinyl)phenyl)-5H-4l4,5l4-dipyrrolo[1,2-c:2',1'-f][1,3,2]diazaborinin-3-amine). The

1 (100 mg, 0.30 mmol) and **5** (100 mg, 0.30 mmol) and were dissolved in 30 mL dry 1,4-dioxane, followed by the addition of Et_3N (0.1 mL) under a nitrogen atmosphere. The reactants were stirred at 80 ℃ for 12 h. The mixture was then evaporated and the residue was dissolved in dichloromethane and extracted (3 x 20 mL). The combined organic layers were washed with water and brine, dried over anhydrous Na_2SO_4, and evaporated under vacuum to afford **TPE-Crimson**, which was purified by means of column chromatography, as a red solid (84 mg, 45%). ^{1}H NMR (600 MHz, $CDCl_3$): δ (ppm) = 8.06 (s, 1H), 7.49-7.45 (m, 5H), 7.13-7.02 (m, 17H), 6.97 (d, *J* = 6 Hz, 2H), 6.89 (d, *J* = 6 Hz, 1H), 6.41 (d, *J* = 6 Hz, 1H), 6.37 (d, *J* = 6 Hz, 1H), 6.22 (d, *J* = 6 Hz, 1H). ^{13}C NMR{^{1}H} (150 MHz, $CDCl_3$): δ (ppm) = 155.7, 140.7, 140.6, 140.5, 139.1, 139.0, 136.9, 132.7, 130.9, 130.8, 130.2, 123.0, 129.3, 128.6, 128.5, 127.6, 126.8, 125.6, 125.1, 125.0, 124.0, 124.0, 123.9, 119.0, 118.6, 110.7, 109.2. EI-MS: m/z = 646.94 $[M]^+$; calculated exact mass: 647.21. Anal. Calcd. for $C_{41}H_{29}BClF_2N_3$: C, 76.00; H, 4.51; N, 6.49. Found: C, 76.19; H, 4.65; N, 6.33.

Synthesis of TPE-NIR ((E)-3,3-dimethyl-1-propyl-2-(4-((4-(1,2,2-triphenylvinyl)phenyl)amino)styryl)-3H-indol-1-ium). The entire process needed to be kept in dark. The **7** (58 mg, 0.17 mmol) and **8** (80 mg, 0.17 mmol) and were dissolved in 20 mL dry ethanol, followed by the addition of pyridine (0.1 mL) under a nitrogen atmosphere. The reactants were stirred at 60 ℃ for 12 h. The mixture was then evaporated under vacuum to afford **TPE-NIR**, which was purified by means of column chromatography, as a blue solid (94 mg, 70%). ^{1}H NMR (600 MHz, DMSO-d_6): δ (ppm) = 9.43 (s, 1H), 8.35 (d, *J* = 18 Hz, 1H), 8.11 (d, *J* = 6 Hz, 2H), 7.82 (s, 2H), 7.57 (d, *J* = 24 Hz, 2H), 7.37 (d, *J* = 12 Hz, 1H), 7.18-6.96 (m, 20H), 4.54 (t, *J* = 6 Hz, 1H), 1.86-1.82 (m, 2H), 1.77 (s, 6H), 0.99 (t, *J* = 6 Hz, 3H). ESI-MS: m/z = 635.38 $[M]^+$;

calculated exact mass: 635.86. Anal. Calcd. for $C_{47}H_{43}IN_2$: C, 74.01; H, 5.68; N, 3.67. Found: C, 74.15; H, 5.77; N, 3.49.

ASSOCIATED CONTENT:

Supporting Information

Optical characteristics of TPEs in the solid and liquid state, single-crystal X-ray diffraction data and their ORTEP drawings of **TPE-Blue** (CCDC 1937424) and **TPE-NIR** (CCDC 1937425), computational data of TPEs, UV−vis absorption spectra, absorption and emission solvatochromism spectra, viscosity emission spectra of TPEs, ^{1}H and $^{13}C\{^{1}H\}$ NMR, MS spectra for TPEs.

Crystallographic information of **TPE-Blue** (CCDC 1937424)

Crystallographic information of **TPE-NIR** (CCDC 1937425)

AUTHOR INFORMATION:

Corresponding author

Jun Yin. Email: yinj@mail.ccnu.edu.cn

Ying Tan. Email: tan.ying@sz.tsinghua.edu.cn

Xie Han. Email: Hanxie@wust.edu.cn

Author contributions

J. Y. and Y. T. designed and supervised the research. X. H. designed, performed experiments and analyzed data. C. Z. partially did experiments, along with a participation in analyzing data. W. C. wrote the manuscript.

Notes

There are no conflicts to declare.

ACKNOWLEDGEMENTS

The authors acknowledge financial support from National Natural Science Foundation of China (21676113, 21402057, 21772054, 21472059); Distinguished Young Scholar of Hubei Province (2018CFA079), Youth Chen-Guang Project of Wuhan (2016070204010098). Supported by the 111 Project B17019; Supported by the Ministry-Province Jointly Constructed Base for State Key Lab-Shenzhen Key Laboratory of Chemical Biology (Shenzhen); Supported by the State Key Laboratory of Materials-Oriented Chemical Engineering (KL17-10); Open Project Fund of Key Laboratory of Natural Resources of Changbai Mountain & Functional Molecules (Yanbian University, NRFM201701), Ministry of Education; Supported by the foundation of Key Laboratory of Synthetic and Biological Colloids, Ministry of Education, Jiangnan University (No. JDSJ2017-07); Supported by self-determined research funds of CCNU from the colleges' basic research and operation of MOE (CCNU18TS012).

REFERENCES

(1) Sharma, A.; Arambula, J. F.; Koo, S.; Kumar, R.; Singh, H.; Sessler, J. L.; Kim, J. S. Hypoxia-targeted drug delivery. *Chem. Soc. Rev.* **2019**, *48*, 771-813.

(2) Liu, Y.; Bhattarai, P.; Dai, Z.; Chen, X. Photothermal therapy and photoacoustic imaging via nanotheranostics in fighting cancer. *Chem. Soc. Rev.* **2019**, *48*, 2053-2108.

(3) Chong, K. C.; Hu, F.; Liu, B. AIEgen bioconjugates for specific detection of disease-related protein biomarkers. *Mater. Chem. Front.* **2019**, *3*, 12-24.

(4) Chen, Y.; Li, L; Chen, W.; Chen, H; Yin, J. Near-infrared small molecular fluorescent dyes for photothermal therapy. *Chin. Chem. Lett.* **2019**, *30*, 1353-1360.

(5) Gu, K.; Zhu, W.-H.; Peng, X. Enhancement strategies of targetability, response and photostability for in vivo bioimaging. *Sci. China Chem.* **2019**, *62*, 189-198.

(6) Zhu, S.; Tian, R.; Antaris, A. L.; Chen, X.; Dai, H. Near-Infrared-II Molecular Dyes for Cancer Imaging and Surgery. *Adv. Mater.* **2019**, *31*, 1900321.

(7) Chen, W.; Pan, Y.; Chen, J.; Ye, F.; Liu, S. H.; Yin, J. Stimuli-responsive organic chromic materials with near-infrared emission. *Chin. Chem. Lett.* **2018**, *29*, 1429-1435.

(8) Gu, B.; Yong, K.-T.; Liu, B. Strategies to Overcome the Limitations of AIEgens in Biomedical Applications. *Small Methods* **2018**, *2*, 1700392.

(9) Jung, H. S.; Verwilst, P.; Sharma, A.; Shin, J.; Sessler, J. L.; Kim, J. S. Organic molecule-based photothermal agents: an expanding photothermal therapy universe. *Chem. Soc. Rev.* **2018**, *47*, 2280-2297.

(10) Wu, D.; Chen, L.; Lee, W.; Ko, G.; Yin, J.; Yoon, J. Recent progress in the development of organic dye based near-infrared fluorescence probes for metal ions. *Coord. Chem. Rev.* **2018**, *354*, 74-97.

(11) Xu, Z.; Chen, J.; Hu, L.-L.; Tan, Y.; Liu S.-H.; Yin, J. Recent advances in formaldehyde-responsive fluorescent probes. *Chin. Chem. Lett.* **2017**, *28*, 1935-1942.

(12) Chen, H.; Dong, B.; Tang, Y.; Lin, W. A Unique "Integration" Strategy for the Rational Design of Optically Tunable Near-Infrared Fluorophores. *Acc. Chem. Res.* **2017**, *50*, 1410-1422.

(13) Sun, W.; Guo, S.; Hu, C.; Fan, J.; Peng, X. Recent Development of Chemosensors Based on Cyanine Platforms. *Chem. Rev.* **2016**, *116*, 7768-7817.

(14) Zhou, J.; Ma, H. Design principles of spectroscopic probes for biological applications. *Chem. Sci.* **2016**, *7*, 6309-6315.

(15) Wu, X.; Zhu, W. Stability enhancement of fluorophores for lighting up practical application in bioimaging. *Chem. Soc. Rev.* **2015**, *44*, 4179-4184.

(16) Yin, J.; Hu, Y.; Yoon, J. Fluorescent probes and bioimaging: alkali metals, alkaline earth metals and pH. *Chem. Soc. Rev.* **2015**, *44*, 4619-4644.

(17) He, X.; Xiong, L.-H.; Zhao, Z.; Wang, Z.; Luo, L.; Lam, J. W. Y.; Kwok, R. T. K.; Tang, B. Z. AIE-based theranostic systems for detection and killing of pathogens. *Theranostics* **2019**, *9*, 3223-3248.

(18) Shen, P.; Zhuang, Z.; Zhao. Z.; Tang, B. Z. AIEgens based on main group heterocycles. *J. Mater. Chem. C* **2018**, *6*, 11835-11852.

(19) Feng, H.-T.; Yuan, Y.-X.; Xiong, J.-B.; Zheng, Y.-S.; Tang, B. Z. Macrocycles and cages based on tetraphenylethylene with aggregation-induced emission effect. *Chem. Soc. Rev.* **2018**, *47*, 7452-7476.

(20) Gopikrishna, P.; Meher, N.; Iyer, P. K. Functional 1,8-Naphthalimide AIE/AIEEgens: Recent Advances and Prospects. *ACS Appl. Mater. Interfaces* **2018**, *10*, 12081-12111.

(21) Yuan, Y.; Liu, B. Visualization of drug delivery processes using AIEgens. *Chem. Sci.* **2017**, *8*, 2537-2546.

(22) Mei, J.; Leung, N. L. C.; Kwok, R. T. K.; Lam, J. W. Y.; Tang, B. Z. Aggregation-Induced Emission: Together We Shine, United We Soar! *Chem. Rev.* **2015**, *115*, 11718-11940.

(23) Islam, Md. M.; Hu, Z.; Wang, Q.; Redshaw, C.; Feng, X. Pyrene-based aggregation-induced emission luminogens and their applications. *Mater. Chem. Front.* **2019**, *3*, 762-781.

(24) Chen, Y.; Lam, J. W. Y.; Kwok, R. T. K.; Liu, B.; Tang, B. Z. Aggregation-induced emission: fundamental understanding and future developments. *Mater. Horiz.* **2019**, *6*, 428-433.

(25) Zhao, J.; Chi, Z.; Yang, Z.; Mao, Z.; Zhang, Y.; Ubba, E.; Chi, Z. Recent progress in the mechanofluorochromism of distyrylanthracene derivatives with aggregation-induced emission. *Mater. Chem. Front.* **2018**, *2*, 1595-1608.

(26) He, Z.; Ke, C; Tang, B. Z. Journey of Aggregation-Induced Emission Research. *ACS Omega* **2018**, *3*, 3267-3277.

(27) Shi, J.; Li, Y.; Li, Q.; Li, Z. Enzyme-Responsive Bioprobes Based on the Mechanism of Aggregation-Induced Emission. *ACS Appl. Mater. Interfaces* **2018**, *10*, 12278-12294.

(28) Zhu, C.; Kwok, R. T. K.; Lam, J. W. Y.; Tang, B. Z. Aggregation-Induced Emission: A Trailblazing Journey to the Field of Biomedicine. *ACS Appl. Bio Mater.* **2018**, *1*, 1768-1786.

(29) Han, X.; Liu, Y.; Liu, G.; Luo, J.; Liu, S. H.; Zhao, W.; Yin, J. A Versatile Naphthalimide–Sulfonamide-Coated Tetraphenylethene: Aggregation-Induced Emission Behavior, Mechanochromism, and Tracking Glutathione in Living Cells. *Chem. Asian J.* **2019**, *14*, 890-895.

(30) La, D. D.; Bhosale, S. V.; Jones, L. A.; Bhosale, S. V. Tetraphenylethylene-Based AIE-Active Probes for Sensing Applications. *ACS Appl. Mater. Interfaces* **2018**, *10*, 12189-12216.

(31) Yang, Q.; Li, D.; Chi, W.; Guo, R.; Yan, B.; Lan, J.; Liu, X.; Yin, J. Regulation of aggregation-induced emission behaviours and mechanofluorochromism of tetraphenylethene through different oxidation states of sulphur moieties. *J. Mater. Chem.* C **2019**, *7*, 8244-8249.

(32) Ma, X.; Hu, L.; Han, X.; Yin, J. Vinylpyridine- and vinylnitrobenzene-coating tetraphenylethenes: Aggregation-induced emission (AIE) behavior and mechanochromic property. *Chin. Chem. Lett.* **2018**, *29*, 1489-1492.

(33) Woo, J.; Kim, G.; Quintero, K.; Hanrahan, M. P.; Palencia, H.; Cao, H. Investigation of desilylation in the recognition mechanism to fluoride by a 1,8-naphthalimide derivative. *Org. Biomol. Chem.* **2014**, *12*, 8275-8279.

(34) Zhao, X.; Yu, C.; Feng, Z.; Yu, Y.; Wang, J.; Hao, E. Wei, Y.; Mu, X.; Jiao, L. Highly Regioselective α-Chlorination of the BODIPY Chromophore with Copper(II) Chloride. *Org. Lett.* **2015**, *17*, 4632-4635.

(35) Kang, N.-Y.; Park, S.-J.; Ang, X. W. E.; Samanta, A.; Driessen, W. H. P.; Ntziachrisots, V.; Vasquez, K. O.; Peterson, J. D.; Yun, S.-W.; Chang, Y.-T. A macrophage uptaking near-infrared chemical probe CDnir7 for in vivo imaging of inflammation. *Chem. Commun.* **2014**, *50*, 6589-6591.

(36) Xu, Z.; Huang, X.; Han, X.; Wu, D.; Zhang, B.; Tan, Y.; Cao, M.; Liu, S. H.; Yin, J.; Yoon, J. A Visible and Near-Infrared, Dual-Channel Fluorescence-On Probe for Selectively Tracking Mitochondrial Glutathione. *Chem* **2018**, *4*, 1609-1628.

(37) Song, F.; Li, Z.; Li, J.; Wu, S.; Qiu, X.; Xi, Z.; Yi, L. Investigation of thiolysis of NBD amines for the development of H_2S probes and evaluating the stability of NBD dyes. *Org. Biomol.* Chem. **2016**, *14*, 11117-11124.

(38) Xiong J.; Wang K.; Yao Z.; Zou B.; Xu J.; Bu X.-H. Multi-stimuli-responsive fluorescence switching from a pyridine-functionalized tetraphenylethene AIEgen. *ACS Appl. Mater. Interfaces* **2018**, *10*, 5819-5827.

(39) Sturala J.; Etherington M. K.; Bismillah A. N.; Higginbotham H. F.; Trewby W.; Aguilar J. A.; Bromley E. H. C.; Avestro A.-J.; Monkman A. P.; McGonigal P. R. Excited-State Aromatic Interactions in the Aggregation-Induced Emission of Molecular Rotors. *J. Am. Chem. Soc.* **2017**, *139*, 17882-17889.

(40) Xiong, J.; Wang, K.; Yao, Z.; Zou, B.; Xu, J.; Bu, X.-H. Multi-Stimuli-Responsive Fluorescence Switching from a Pyridine-Functionalized Tetraphenylethene AIEgen. *ACS Appl. Mater. Interfaces* **2018**, *10*, 5819-5827.

(41) Liu, F.; Tu, J.; Wang, X.; Wang, J.; Gong, Y.; Han, M.; Dang, X.; Liao, Q.; Peng, Q.; Li, Q.; Li, Z. Opposite mechanoluminescence behavior of two isomers with different linkage positions. *Chem. Commun.* **2018**, *54*, 5598-5601.

(42) Ma, Z.; Wang, Z.; Meng, X.; Ma, Z.; Xu, Z.; Ma, Y.; Jia, X. A Mechanochromic Single Crystal: Turning Two Color Changes into a Tricolored Switch. *Angew. Chem. Int. Ed.* **2016**, *55*, 519-522.

(43) Qi, Q.; Qian, J.; Tan, X.; Zhang, J.; Wang, L.; Xu, B.; Zou, B; Tian, W. Remarkable Turn-On and Color-Tuned Piezochromic Luminescence: Mechanically Switching Intramolecular Charge Transfer in Molecular Crystals. *Adv. Funct. Mater.* **2015**, *25*, 4005-4010.

(44) Gong, Y.; Tan, Y.; Liu, J.; Lu, P.; Feng, C.; Yuan, W. Z.; Lu, Y.; Sun, J. Z.; He, G.; Zhang, Y. Twisted D-π-A solid emitters: efficient emission and high contrast mechanochromism. *Chem. Commun.* **2013**, *49*, 4009-4011.

(45) Wang, J.; Mei, J.; Hu, R. Sun, J. Z.; Qin, A.; Tang, B. Z. Click Synthesis, Aggregation-Induced Emission, E/Z Isomerization, Self-Organization, and Multiple Chromisms of Pure

Stereoisomers of a Tetraphenylethene-Cored Luminogen. *J. Am. Chem. Soc.* **2012**, *134*, 9956-9966.

(46) Zhao, W.; He, Z.; Peng, Q.; Lam, J. W. Y.; Ma, H.; Qiu, Z.; Chen, Y.; Zhao, Z.; Shuai, Z.; Dong, Y.; Tang, B. Z. Highly sensitive switching of solid-state luminescence by controlling intersystem crossing. *Nat. Commun.* **2018**, *9*, 3044.

(47) Wang, C.; Yu, Y.; Chai, Z.; He, F.; Wu, C.; Gong, Y.; Han, M.; Li, Q.; Li, Z. Recyclable mechanoluminescent luminogen: different polymorphs, different self-assembly effects of the thiophene moiety and recovered molecular packing via simple thermal-treatment. *Mater. Chem. Front.* **2019**, *3*, 32-38.

Graphic Abstract